Multiaxial mechanical behavior of human fetal membranes and its relationship to microstructure

Originally published in:
Biomechanics and Modeling in Mechanobiology 12(4), https://doi.org/10.1007/s10237-012-0438-z

Biomech Model Mechanobiol (2013) 12:747–762
DOI 10.1007/s10237-012-0438-z

ORIGINAL PAPER

Multiaxial mechanical behavior of human fetal membranes and its relationship to microstructure

W. Buerzle · C. M. Haller · M. Jabareen · J. Egger · A. S. Mallik · N. Ochsenbein-Koelble · M. Ehrbar · E. Mazza

Received: 5 April 2012 / Accepted: 30 August 2012 / Published online: 13 September 2012

Abstract This study was directed to the measurement of the mechanical response of fetal membranes to physiologically relevant loading conditions. Characteristic mechanical parameters were determined and their relation to the microstructural constituents collagen and elastin as well as to the pyridinium cross-link concentrations analyzed. 51 samples from twelve fetal membranes were tested on a custom-built inflation device, which allows mechanical characterization within a multiaxial state of stress. Methods of nonlinear continuum mechanics were used to extract representative mechanical parameters. Established biochemical assays were applied for the determination of the collagen and elastin content. Collagen cross-link concentrations were determined by high-performance liquid chromatography measurements. The results indicate a distinct correlation between the mechanical parameters of high stretch stiffness and membrane tension at rupture and the biochemical data of collagen content and pyridinoline as well as deoxypyridinoline concentrations. No correlation was observed between the mechanical parameters and the elastin content. Moreover, the low stretch stiffness is, with a value of $105 \pm 31 \times 10^{-3}$ N/mm much higher for a biaxial state of stress compared to a uniaxial stress configuration. Determination of constitutive model equations leads to better predictive capabilities for a reduced polynomial hyperelastic model with only terms related to the second invariant, I_2, of the right Cauchy-Green deformation tensor. Relevant insights were obtained on the mechanical behavior of fetal membranes. Collagen and its cross-linking were shown to determine membrane's stiffness and strength for multiaxial stress states. Their nonlinear deformation behavior characterizes the fetal membranes as I_2 material.

Keywords Fetal membrane · Biaxial response · Collagen · Elastin · Cross-links

W. Buerzle · E. Mazza (✉)
Department of Mechanical and Process Engineering,
Swiss Federal Institute of Technology, Zurich, Switzerland
e-mail: mazza@imes.mavt.ethz.ch

C. M. Haller · N. Ochsenbein-Koelble · M. Ehrbar
Clinic of Obstetrics, University Hospital Zurich,
Zurich, Switzerland

E. Mazza
Swiss Federal Laboratories for Materials Science and Technology,
EMPA Duebendorf, Duebendorf, Switzerland

M. Jabareen
Faculty of Civil and Environmental Engineering, Technion,
Israel Institute of Technology, Haifa, Israel

J. Egger
Department of Information Technology and Electrical
Engineering, Swiss Federal Institute of Technology,
Zurich, Switzerland

A. S. Mallik
Division of Surgical Research, University Hospital Zurich,
Zurich, Switzerland

1 Introduction

The fetal membrane (FM) is a membranous structure that surrounds and protects the developing fetus during gestation and is composed of two layers, called amnion and chorion. During pregnancy, the membrane deforms as a consequence of internal pressure as well as fetal movements. The rupture of the FM is an integral part of term delivery but has serious complications when it happens prior to term. The spontaneous preterm premature rupture of the FM (PPROM) affects 3 % of all pregnancies worldwide (Calvin and Oyen 2007;

Mercer 2003) and is associated with a high risk for perinatal morbidity and mortality. In addition, iatrogenic PPROM is the Achilles heel in the field of developments for minimally invasive fetal surgery, which occurs in about 30 % of all treatments (Beck et al. 2011). The development of future treatments to prevent premature rupture requires understanding the mechanical behavior and failure of fetal membranes and its relationship to membrane's microstructure.

The macroscopic anatomy of the FM distinguishes two layers, amnion and chorion, where amnion is the inner layer facing the amniotic fluid and chorion the outer layer facing the uterine wall (Ilancheran et al. 2009). Membranes at term present an amnion layer with thickness in the range of 100 μm and significantly higher stiffness and strength, as compared with the chorion, which is 300–500 μm thick, compliant and extensible. Amnion and chorion are further subdivided into sub-layers of different cellular content and fibrous components of the extracellular matrix (Ilancheran et al. 2009). The mechanical properties of the membrane are commonly related to the type and distribution of collagen in the connective tissue. Amnion contains fibrils forming collagen types I and III in all layers below the amniotic epithelium, along with filamentous collagen types V and VI, which contribute to connecting the fibrillar components to the surrounding connective tissue (Malak et al. 1993); collagen type IV is present in the amniotic basement membrane and contributes to an anchoring zone between amniotic mesoderm and epithelium (Bachmaier and Graf 1999). Chorion contains fibrillar collagen in the reticular layer, interfacing amnion, and collagen type IV in the trophoblast layer. The latter provides the scaffold for the assembly of other non-collagen structural proteins (laminin, entacin, and proteoglycan), (Bryant-Greenwood 1998). Measurement of the FM total collagen content has been reported, providing contents of 4–20 % (Hampson et al. 1997; Jabareen et al. 2009) of dry weight. Not only fibrillar collagen quantity, but also its cross-linking and fibrils arrangement determines tissue's strength and stiffness. Protocols for quantitative determination of pyridinium cross-links (relevant to fibril forming collagen) are available as part of an established method for the diagnosis of osteoporosis. So far, measurements were taken in one single study of human amnion. Stuart et al. (2005) report values of the pyridinoline (PYD) and deoxypyridinoline (DPD, in Avery and Bailey (2008) referred to as hydroxyllysil–pyridinoline) concentrations and conclude that collagen cross-linking is not involved in the etiology of PROM. Meinert et al. (2001) attributed a relevant role in the mechanical stability of amnion to the proteoglycan decorin, which binds to collagen type I and III, and facilitates the lateral alignment or organization of collagen fibrils.

Elastin also contributes to the deformation behavior of FM. Determination of the elastin content in FM is challenging and has only been achieved in recent studies. The published values ranging from 0.08 % of fat-free dry weight (Hieber et al. 1997) to approximately 2 % of wet weight (Jabareen et al. 2009), up to 36 % of (total) wet weight of fresh amnion (Wilshaw et al. 2006) point at the difficulties involved in the quantitative determination of elastin in fetal membranes.

Information on the ultrastructure of the membrane is available from electron microscopy studies. Scanning electron micrographs of the amnion in cross-section demonstrated a composite layered structure (Oyen et al. 2005). Distinct layers can be observed, including a surface cell layer and a collagen network with varying density, with greatest density immediately beneath the cell layer (compact layer). The collagen network appears to be mainly oriented in the membrane plane. Electron microscope images of amnion in Hollenstein (2011) show individual collagen fibrils approximately 50 nm in diameter, organized in somewhat loose bunches, which appears randomly interwoven without perceivable directionality. Assembly of the collagen fibrils into higher-order bundles has not been observed.

In the last decades, many experiments were conducted to understand FM mechanics and failure and its relation to membranes structure and morphology (Moore et al. 2006; El Khwad et al. 2005). Most studies were aimed to the determination of the rupture strength to get insight into the mechanisms leading to PROM (Artal et al. 1976; Lavery and Miller 1979). Other studies were performed in order to determine the different mechanical properties of amnion and chorion (Oxlund et al. 1990). Three types of mechanical test setups were used for these purposes: (i) uniaxial tensile test (Oxlund et al. 1990; Helmig et al. 1993; Jabareen et al. 2009), which is rather simple to perform and to analyze but does not represent the physiological conditions of loading, (ii) puncture testing (Joyce et al. 2009 and references therein), where a spherical metal probe is used to deflect the clamped circular membrane specimen, and (iii) inflation or burst testing (Al-Zaid et al. 1980; Lavery and Miller 1979; Polishuk et al. 1962; Wittenberg 2011), where a circular membrane is deformed with the aid of pressurized water or air. Puncture testing allows characterizing a large number of samples in each FM, but the local force application leads to a state of deformation that differs from the in vivo loading condition. Nevertheless, Schober et al. (1994b) has shown that results obtained by puncture testing can be related to results from inflation tests. Membrane inflation best mimics the physiological loading situation and the in vivo mechanical deformation. Burst tests were accomplished to acquire data on rupture properties of FM, such as burst pressure (MacLachlan 1965) or elevation at rupture (Parry-Jones and Priya 1976). Other studies compared the rupture properties of term membranes with those of preterm ruptured membranes (Lavery and Miller 1979; Al-Zaid et al. 1980) or the difference in the rupture properties between vaginally delivered membranes and membranes

from caesarean sections (Lavery et al. 1982). Most investigations provide system parameters (e.g., burst pressure, which depends on sample geometry) instead of specific properties of FM. Fewer studies also determined material-specific rupture properties, such as critical membrane tension or critical stress (Lavery and Miller 1979; Lavery et al. 1982; Polishuk et al. 1962). Schober et al. (1994a) provided also information on the deformation behavior in inflation experiments, in that he calculated the slope (tangent stiffness) at the end of the pressure–elevation curve. Apart from the foregoing mentioned three types of mechanical testing, planar biaxial testing is a further common method for multiaxial characterization of materials. Joyce (2009) has recently applied it to fetal membranes and determined nonlinear stress–strain curves as well as the maximum tangent modulus and the maximum membrane tension. Miller et al. (1979) were the first who determined parameters for a nonlinear constitutive model (Mooney material) based on inflation testing. Prevost (2004) (uniaxial and inflation tests), Joyce (2009) (planar biaxial tests) and Jabareen et al. (2009) (uniaxial tensile tests) proposed a nonlinear constitutive model for the mechanical response of FM. No other quantitative information characterizing the nonlinear stress–strain response of FM in a biaxial state of stress can be found in the literature.

Our previous study (Jabareen et al. 2009) for the first time reported data on the nonlinear deformation behavior related to the elastin and collagen content of the same FM. The present work represents a continuation along this line and provides data from 51 inflation experiments on human FM linked with corresponding determination of microstructural data. The aim of this study was to characterize FM mechanical response in a biaxial state of stress (using an own-built system for FM inflation experiments) and to correlate the biaxial mechanical parameters with elastin and collagen content as well as with the amount of collagen cross-links. Nonlinear continuum mechanics models were used for the analysis of the tension–stretch curves of each sample, and biochemical assays were applied to determine the weight percentage of collagen and elastin as well as the amount of DPD and PYD cross-links in the same fetal membrane.

2 Materials and methods

2.1 Sample collection and sample preparation

Fetal membranes were collected from patients with single child pregnancies who underwent elective cesarean sections between 37 and 40 weeks of gestation, the obstetric parameters can be found in Table 1. Patients were recruited for this study with informed written consent according to the protocol approved by the Ethical Committee of the District of Zurich (study Stv22/2006). The patients were randomly selected for this study after negative testing for HIV, hepatitis B, and streptococcus B. The selected pregnancies had no history of diabetes, connective tissue disorders, or chromosomal abnormalities. The membranes were cut approximately 2 cm away from the placental border and stored in saline solution until mechanical testing within a few hours after delivery. It should be noted that the FM samples included parts of the maternal decidua. The main cellular layer might thus be referred to as choriodecidua. Due to logistic reasons, four membranes were frozen at −20 °C for one day before mechanical testing. Analysis of the mechanical and histological tests revealed no significant difference in the fresh samples for which reason also the frozen membrane samples were included in the analysis of this campaign.

Table 1 Obstetric parameters: patient's age, gestational age (GA), and number of samples (N) for mechanical testing per membrane

Membrane	Age (year)	GA (week + day)	N (–)
1	20	38 + 4	4
2	32	38 + 2	6
3	36	38 + 6	4
4	36	38 + 2	4
5	28	39 + 2	3
6	27	37 + 4	5
7	41	37 + 2	4
8	34	37 + 3	4
9	29	37 + 0	5
10	34	38 + 2	5
11	42	38 + 2	3
12	46	38 + 4	4

To generate samples for mechanical testing, FM was gently spread out on a plastic mat and sandpaper rings (3M, wetordry P400), with an inner diameter of 50 mm and an outer diameter of 70 mm, were glued (UHU, super glue) on each side of the membrane, see Fig. 2a. The sandpaper rings allowed to maintain the tissue in a relaxed state during handling and considerably improved gripping so to avoid slippage within the clamping device of the inflation experiment. After preparation, the samples were stored in saline solution until mechanical testing to prevent dehydration.

2.2 Experimental setup

With the aim of measuring the mechanical response of FM in a biaxial, close to physiologic loading configuration, a dedicated inflation device was developed, see Fig. 1a. The circular sample, supported through the sandpaper rings, is placed, with the amnion side facing downwards, on a fluid-filled cylinder and fixed using a clamping ring with 50 mm inner diameter, see Fig. 2. Saline solution is pumped into the cylinder with the aid of a peristaltic pump (type 314VBM, four

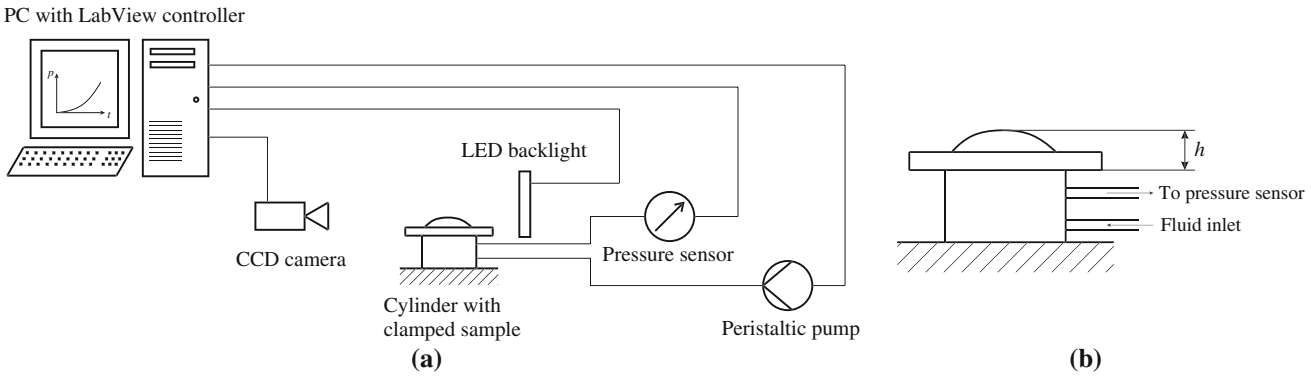

Fig. 1 Experimental setup. **a** A circular membrane sample is inflated with the aid of a peristaltic pump which conveys saline solution from the lower standing fluid reservoir. The pressure inside the cylinder is measured and controlled by a LabView code to follow a desired pressure profile. A CCD camera records images and a red LED backlight is installed behind the sample to improve the contrast of the images. **b** Schematic drawing of the cylinder with the inflated membrane. The measure h indicates the height of the fluid column with respect to the level where the membrane is clamped and the pressure is zeroed at the beginning of the measurement

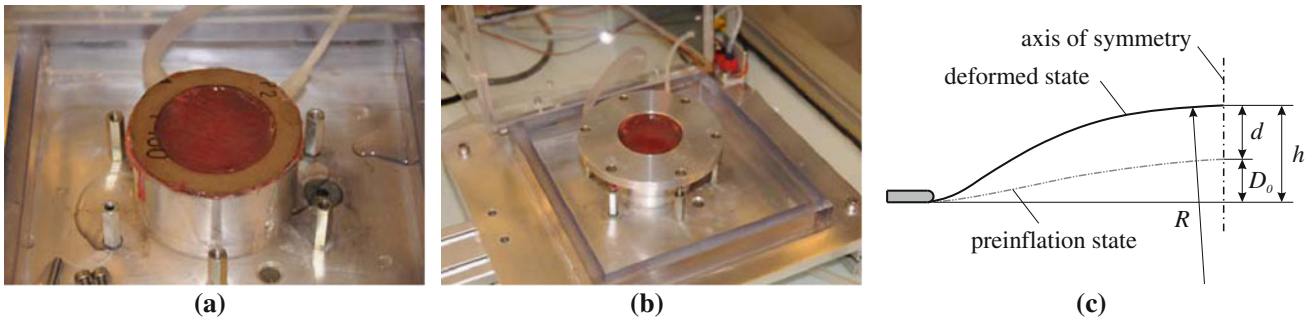

Fig. 2 **a** Sandpaper rings are glued on both side of the FM sample to stabilize the sample during handling and to improve soft tissue gripping. **b** The sample is fixed using a clamping ring with 50 mm inner diameter. **c** Schematic drawing of an inflated membrane with indication of geometrical quantities

rollers, Watson-Marlow Ltd., Zurich, Switzerland). During the test, the pressure (digitale manometer, LEX 1, accuracy 0.05 %, Keller, Winterthur, Switzerland) within the cylinder is measured and pictures from the side view profile (Model Dragonfly2, resolution 640 × 480 pixel, 1/3″ CCD, Point Grey, Vancouver BC, Canada) of the deformed membrane are simultaneously registered. To improve the contrast of the images, a red LED backlight (Moritex, MEBL CR7050, Fujifilm AG, Dielsdorf, Switzerland) was mounted behind the cylinder. The system for image acquisition and analysis is calibrated at the beginning of each measurement series. The test is executed under a pressure-controlled regime with a rate of pressure increase of 0.65 mbar/s. Saline solution is at room temperature, and no temperature control is included in the present system. Monotonic pressure increase continues until membrane bursting. The typical duration of each experiment is 4 min. During this time, the outer surface of the membrane is sprayed with saline solution to avoid dehydration. The whole system is controlled by a LabView code (LabView 2008). The experimental data used for further analysis consist of the pressure time history and the corresponding image series of the deformed membrane profile.

2.3 Image analysis

Analysis of the recorded calibration images and experimental image series is used to quantify the deformation of the membrane. The image analysis procedure has three main goals: (i) determination of the mm-pixel calibration ratio, (ii) measurement of the apex displacement, and (iii) extraction of the radius of curvature of the inflated membrane. To analyze the images, the MATLAB intrinsic function edge, using the so-called Canny method (Canny 1986) for edge detection, (MATLAB 2010), is applied.

A ball of known diameter is placed in the cylinder to generate a calibration picture. The edge extraction algorithm delivers the contour of the reference sphere. Comparison of the sphere dimensions with the corresponding data in the pixel space allows determining the mm-pixel ratio, typically in the range of 0.1 mm/pixel. The apex position is obtained by measuring the position of the highest point of the inflated

membrane with respect to the upper surface of the fluid-filled cylinder. Since the clamping ring has a thickness of 1 mm, displacements below this value cannot be detected. The radius of curvature R is determined by the analysis of a region of ± 100 pixel from the axis of the cylinder, see Fig. 2c. The edge contour points within this region are used to fit a circular arc, thus providing R, the radius of this arc. For each experiment, the image analysis procedure determines the time histories of displacement and radius, $d(t)$ and $R(t)$, respectively, see Fig. 2c. Typical sampling rates are in the order of one image every 125 ms.

2.4 Normalization

The pressure p_{tot} measured inside of the fluid-filled cylinder during membrane inflation results from two contributions: the hydrostatic pressure p_{hydr} due to the increasing fluid column and the pressure due to the resistance of the stretched membrane p_{memb}.

$$p_{\text{tot}} = p_{\text{hydr}} + p_{\text{memb}} \tag{1}$$

The hydrostatic pressure contribution is given by the law of Bernoulli:

$$p_{\text{hydr}} = \rho g h \tag{2}$$

where g is the gravitational constant, ρ the density of the fluid, and h the height of the fluid column, see Fig. 1b. Since the pressure is zeroed at the beginning of the measurement, the height h refers to the level where the sample is clamped. The clamped membrane sample is initially slack with irregular wrinkles, and the initial resistance to inflation is negligible. Thus, we define the beginning of the measurement at the time point for which the membrane starts to oppose measurable resistance to elevation, that is, when the difference between the measured total pressure and the hydrostatic pressure

$$p_{\text{diff}} = p_{\text{tot}} - p_{\text{hydr}} \tag{3}$$

reaches a threshold value. For the present setup and pressure sensor resolution, a threshold value of 1 mbar was selected. Similar to Myers et al. (2010), this procedure was introduced in order to obtain a repeatable definition of the reference configuration for the analysis of each experiment. This so-called preinflation state corresponds to a slightly distended condition of the membrane and differs considerably from the slack state of the initially clamped membrane. All measured data are set to zero with respect to this reference state, and the pressure difference $p_{\text{diff}} = 1$ mbar is the preload. The reference geometry is characterized by the corresponding "preinflation displacement" D_0, see Fig. 2c. Note that none of the previously reported experimental investigations using inflation experiments included such an analysis for the determination of the reference state, which was shown to have a significant influence on the measurement results, see Sect. 4.6.

2.5 Tension calculation

The membrane is stretched in radial and circumferential direction and contracts in thickness direction with respect to the axisymmetric reference configuration of the inflation test. For a homogeneous membrane, the stress field ranges from a so-called pure-shear configuration, Ogden (1972), at the clamping site to the equibiaxial stress state at the apex position. This study focuses on the characterization of FM behavior under equibiaxial stress. Thus, only the apex region is considered for the analysis of tension–stretch response. Since the membrane thickness is much smaller than the sample size, a plane stress state is assumed. Further, the membrane is considered as isotropic in its plane (in fact, no anisotropy could be observed in uniaxial or multiaxial experiments in our laboratory as well as in planar biaxial tests by Joyce et al. (2009)). The membrane tension T at the apex can be calculated based on force equilibrium (Laplace's law) as a function of the internal pressure p (membrane's pressure load p_{memb}) and the radius of curvature R for each timestep t of the recorded image series:

$$T = \frac{p(t)R(t)}{2} \tag{4}$$

It is well known that the two major constituent layers of the fetal membrane, amnion and chorion, possess different mechanical properties (Oxlund et al. 1990). Amnion is known to be stiffer, stronger, and thinner than chorion. Testing intact FM samples causes an inhomogeneous stress distribution along the sample thickness. For this reason, stress is not an adequate measure for the mechanical characterization of intact FM samples. Correspondingly, in the present work, we characterize FM as a structure (membrane) and not as a material.

2.6 Stretch model

With the current experimental setup, no direct measurement of the stretch in the equibiaxial region is taken. Comparison between reference and current images provides an integral measure of membrane's profile deformation. An approach based on the finite element (FE) method was chosen to assess the time history of stretch $\lambda_{\text{plane}}(t)$ in the apex region. So-called stretch curves, describing $\lambda_{\text{plane}}(t)$ as a function of the apex displacement $d(t)$, were calculated based on FE simulations and parameterized to get a mathematical representation to assign the equibiaxial stretch to the measured apex displacement.

The FE simulation consists of two steps. The first step, called "preinflation," starts from an initially flat membrane.

The pressure load is applied and the maximum pressure magnitude varied to achieve the deformed reference configuration, characterized by the apex displacement value D_0. Once this target displacement is achieved, the nodal stresses and strains are set to zero. In this way, the nodal position at the end of the first step represents the reference configuration ("pre-inflation state") for the following membrane inflation simulation. In this second step, the pressure magnitude is increased, leading to growing apex displacement up to $d = 15\,\text{mm}$. The FE software ABAQUS 6.6-3 (ABAQUS 2006) in combination with MATLAB R2010a (MATLAB 2010) was used for these simulations. The FE model consists of 270 axisymmetric 4-node solid elements (element type CAX4RH). Geometric and material nonlinearities are considered. Dissipative behavior is neglected for the present analysis (assuming that the observed FM deformation corresponds to the long-term response of the material). Different (incompressible) hyperelastic constitutive model formulations are implemented to represent the nonlinear material behavior. In fact, evaluation of the FM response in one single experimental configuration does not provide sufficient information to uniquely identify a representative strain energy functional form. Calculations using different model equations were performed in order to investigate the influence of the constitutive model formulation on the extraction of FM mechanical parameters as well as on the corresponding correlations with microstructural data. The implemented constitutive models are (i) a three-parameter reduced polynomial form (Rivlin and Saunders 1951),with the strain energy expressed as a function of the second invariant I_2 of the right Cauchy-Green deformation tensor $\mathbf{C}$ (i.e., the coefficients of I_1 are set to zero), (ii) the Rubin–Bodner model (Rubin and Bodner 2002), based on the first invariant I_1 of $\mathbf{C}$, and (iii) the Ogden model (Ogden 1972), with the strain energy as a function of the principal stretches. The mathematical formulation of the strain energy associated with each model as well as the used set of parameters can be found in Table 2. Note, the Rubin–Bodner model formulation when restricted to isotropic elastic incompressible behavior is akin to the formulation proposed in Demiray (1972).

Simulations were carried out for a set of preinflation displacements $D_0 = \{0, 4, 8, 12, 16, 20, 24\}\,\text{mm}$. The plane stretch λ_{plane} as a function of the apex displacement is determined from the FE calculation and represented as polynomial function:

$$\lambda_{\text{plane}}(d, D_0) = 1 + C_1(D_0)d + C_2(D_0)d^2 + C_3(D_0)d^3 \tag{17}$$

Table 3 lists the expressions of the corresponding coefficients $C_1(D_0)$, $C_2(D_0)$ and $C_3(D_0)$, and Fig. 3 illustrates the corresponding curves for all implemented constitutive models.

Table 2 Implemented constitutive models and corresponding set of parameters, given in (N/mm) (except α_p and q which are dimensionless)

Reduced polynomial	
$\Psi_m = \sum_{j=1}^{3} C_{0j}(I_2 - 3)^j$	(5)
$C_{01} = 2.24 \times 10^{-6}$	(6)
$C_{02} = 1.30 \times 10^{-2}$	(7)
$C_{03} = 0.402$	(8)
Rubin Bodner	
$\Psi_m = \frac{\mu_0}{2q}[e^{qm_2(I_1-3)} - 1]$	(9)
$\mu_0 = 2.88 \times 10^{-3}$	(10)
$q = 1.75$	(11)
$m_2 = 3.43$	(12)
Ogden	
$\Psi_m = \sum_{p=1}^{3} \frac{\mu_p}{\alpha_p}(\lambda_1^{\alpha_p} + \lambda_2^{\alpha_p} + \lambda_3^{\alpha_p} - 3)$	(13)
$\mu_1 = 3.15 \times 10^{-6}, \quad \alpha_1 = 28.3$	(14)
$\mu_2 = 8.53 \times 10^{-4}, \quad \alpha_2 = 10.5$	(15)
$\mu_3 = 3.39 \times 10^{-4}, \quad \alpha_3 = 15.1$	(16)

The model formulations have been adapted for a uniform expression. Model parameters are reported for a membrane model formulation Ψ_m: strain energy per unit reference area of the membrane midplane surface

2.7 Analysis of tension–stretch curves

The fetal membrane tissue undergoes large deformations and exhibits distinct nonlinearity in the pressure–displacement as well as in the tension–stretch relation, often denoted as bilinear behavior. Two scalar parameters, the low stretch modulus K_1 and the high stretch modulus K_2, are determined in order to characterize this bilinear behavior in each curve of tension versus plane stretch. The values are calculated from the initial and final 10 % of the curves obtained from calculations based on the measured time histories of pressure and apex displacement. The strength of the membrane tissue is determined as the membrane tension at rupture. The rupture of

Table 3 Constitutive models and coefficients for the parameterization of the stretch curves, see Eq. 17

Reduced polynomial	
$C_1 = 1.41 \times 10^{-2} + 1.92 \times 10^{-3} D_0 - 4.32 \times 10^{-5} D_0^2$	(18)
$C_2 = 6.67 \times 10^{-4} - 4.34 \times 10^{-5} D_0 + 5.92 \times 10^{-7} D_0^2$	(19)
$C_3 = 0$	(20)
Rubin Bodner	
$C_1 = 8.25 \times 10^{-4} + 2.21 \times 10^{-3} D_0 - 5.65 \times 10^{-5} D_0^2$	(21)
$C_2 = 8.20 \times 10^{-4} - 4.41 \times 10^{-5} D_0 + 8.48 \times 10^{-7} D_0^2$	(22)
$C_3 = 0$	(23)
Ogden	
$C_1 = -1.55 \times 10^{-3} + 2.68 \times 10^{-3} D_0 - 9.09 \times 10^{-5} D_0^2$	(24)
$C_2 = 1.26 \times 10^{-3} + 2.51 \times 10^{-5} D_0 + 2.16 \times 10^{-6} D_0^2$	(25)
$C_3 = 1.34 \times 10^{-6} - 2.62 \times 10^{-6} D_0 - 6.31 \times 10^{-8} D_0^2$	(26)

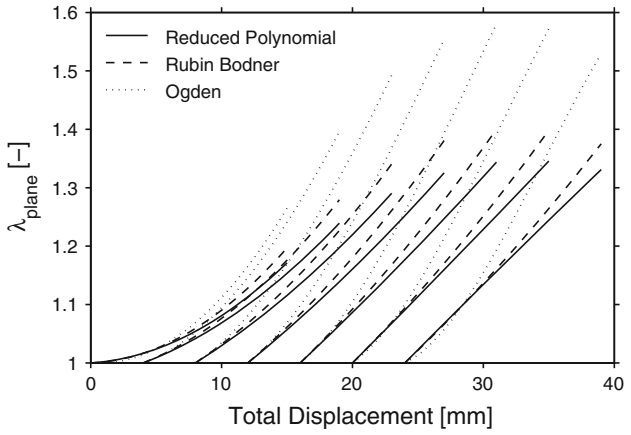

Fig. 3 Stretch curves obtained from different constitutive models as a function of total displacement = preinflation displacement D_0 + further apex displacement d. *Continuous line*: Reduced polynomial model, *dashed line*: Rubin Bodner model and *dotted line*: Ogden model

the membrane is characterized by a sudden decrease in the pressure value due to fluid leakage through a local defect. In case of a gradual rupture, membrane failure is identified by the first distinct pressure drop. Thus, in both cases, failure coincides with the time point of the value p_1 in Fig. 5. Careful visual inspection allows to identify the rupture position and sequence. In addition, the corresponding pressure histories are analyzed to associate characteristic $p(t)$ patterns to the observed rupture sequence. For the determination of the strength, only the samples which ruptured in the free area (no rupture at or close to the clamping) are taken into account. In summary, four mechanical parameters were extracted from the tension–stretch curves: low and high stretch stiffness K_1 and K_2, critical membrane tension T_{crit} and ductility λ_{crit}.

2.8 Biochemical assays

Biochemical assays enable the quantitative determination of the total collagen and elastin content. The procedure for the determination of elastin content has been described in Jabareen et al. (2009). Insoluble elastin is quantified from membrane samples as soluble cross-linked polypeptides by oxalic acid extraction. Lyophilized tissue is extracted in oxalic acid, and the amount of soluble elastin is determined colorimetrically using a Fastin Elastin assay kit (Biocolor Ltd., Newtonabbey, Northern Ireland) following the manufacture's instruction.

For the estimation of the total collagen, an acid hydrolysis method is applied to determine the hydroxyproline. Lyophilized tissue is hydrolyzed with hydrochloric acid, and hydrolyzed collagen is converted to pyrrole-2-carboxylic acid. Further reaction gives the amount of hydroxyproline, a red discolored product, whose absorbance is measured at 540 nm.

Measurement of the two collagen cross-links pyridinoline (PYD) and deoxypyridinoline (DPD) was taken at The Institute for Clinical Chemistry and Hematology, University Hospital St. Gallen, Switzerland. Cross-links were determined by high-performance liquid chromatography (HPLC). The first step of the analysis is the hydrolyzation of the tissue samples. After dilution, the mixture is loaded on an extraction tube. After a washing step, the pyridinium cross-links PYD and DPD are eluted from the extraction tube. The separation of PYD and DPD on the HPLC system is based on the ion pair chromatography on a reversed phase cartridge with isocratic elution. Detection is achieved by their natural fluorescence.

The biochemical analyses are carried out on three samples per membrane from the material left over after extraction of the samples used for the mechanical tests.

2.9 Statistical analysis

Data of collagen and elastin content, amnion and chorion thickness as well as the mechanical parameters are presented as mean ± SD. Coefficients of correlation are calculated using the built-in function of MATLAB. Statistical significance of the coefficients of correlation is evaluated by a two-tailed t test. Results are considered to be statistically significant if the p value is smaller than 0.05.

3 Results

3.1 FM response to biaxial inflation

A total of 51 samples from 12 membranes have been tested using the inflation device. Figure 4a shows the pressure versus displacement curves for the samples of one membrane after normalization according to Sect. 2.4. The averaged pressure–displacement curves of all 12 membranes are illustrated in Fig. 4b. As can been seen in Fig. 4, there is a pronounced variability within the samples of the same membrane and a somewhat larger variability among averaged curves of the membranes from different donors. All curves are characterized by a low initial stiffness followed by a transition region leading to an almost linear pressure–displacement relation for large displacements.

Overall averaged data were determined in order to characterize the present inflation experiments: D_0 is 15.3 ± 2.7 mm, the maximum pressure and displacement at rupture of the membrane are 152.3 ± 50.6 mbar and 9.0 ± 1.6 mm, respectively (note that for the latter values, only the 38 samples which ruptured away from the clamping were considered).

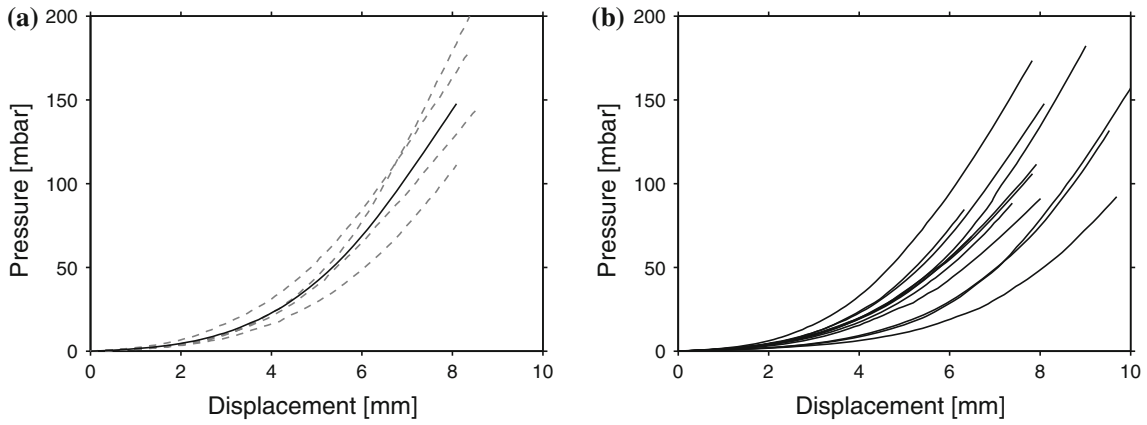

Fig. 4 Pressure–displacement graphics for the four samples of membrane 5 plus average curve (**a**) and average pressure–displacement curves for all tested membranes (**b**)

Table 4 Microstructural data: collagen and elastin content in percentage per dry weight (DW) and amount of pyridinium cross-links PYD and DPD

Collagen, elastin, and cross-link measurements were taken on three samples for each membrane from the material left over after extraction of the samples used for mechanical testing. Thickness was measured sample specific after mechanical testing

Membrane	Collagen (% DW)	Elastin (% DW)	PYD (nmol/l)	DPD (nmol/l)	Thickness (μm)
1	21.9 ± 0.2	19.0 ± 2.3	10,976 ± 410	677 ± 108	608 ± 152
2	25.6 ± 0.0	16.6 ± 2.8	9,569 ± 2,589	457 ± 146	263 ± 117
3	21.7 ± 1.3	17.0 ± 1.8	7,071 ± 1,144	359 ± 50	451 ± 288
4	9.9 ± 0.2	16.9 ± 0.7	3,509 ± 808	131 ± 37	644 ± 101
5	18.5 ± 0.2	16.9 ± 1.7	7,071 ± 1,062	364 ± 73	453 ± 19
6	16.9 ± 0.8	15.6 ± 0.9	3,179 ± 1,228	153 ± 105	545 ± 167
7	17.3 ± 1.1	18.0 ± 1.1	3,556 ± 255	187 ± 18	561 ± 255
8	17.1 ± 1.2	16.2 ± 2.2	2,654 ± 544	89 ± 22	437 ± 139
9	15.1 ± 0.9	17.4 ± 2.2	2,266 ± 25	97 ± 19	541 ± 117
10	12.6 ± 0.8	21.4 ± 0.8	1,502 ± 582	39 ± 14	697 ± 195
11	18.0 ± 1.0	15.8 ± 2.3	2,070 ± 804	87 ± 27	487 ± 139
12	26.2 ± 3.5	20.7 ± 2.8	3,774 ± 886	162 ± 42	430 ± 108

3.2 Histology and biochemical characteristics

Table 4 summarizes the microstructural data of the 12 tested membranes. Resulting from the histological assays, the contents of the microstructural constituents are given as mg of collagen or elastin per g dry weight of the tissue sample and converted to % per dry weight (DW). Average contents of collagen and elastin ($N = 12$) are $18.4 \pm 4.9\,\%$ DW, and $17.6 \pm 1.9\,\%$ DW, respectively. The amount of the pyridinium cross-links PYD and DPD was determined by HPLC method. Average content ($N = 12$) of PYD is $4{,}766 \pm 3{,}125$ nmol/l and DPD 233 ± 191 nmol/l, giving an average PYD/DPD ratio of 23.8 ± 5.7.

3.3 Rupture sequence and position

Different rupture sequences (amnion first vs. chorion first) and different positions of initiation of rupture were observed during the test. In 37 cases, amnion ruptured before chorion (in 11 cases with fluid leaking through amnion and separating the two layers). Chorion ruptured before amnion in only eight cases. For six samples, both layers ruptured simultaneously. In addition to the visual assessment of the rupture sequence, also the pressure histories were analyzed. Figure 5 illustrates two characteristic pressure courses. Rupture of the membrane is characterized by a sudden decrease in the pressure value which reached a first maximum p_1. If only one layer of the membrane ruptured, a subsequent increase in the pressure can be observed which reaches a second maximum p_2. Two characteristic cases can be distinguished: if amnion ruptures first, the second maximum is clearly smaller than the first $p_1 > p_2$. In contrast, there is a pronounced increase in the pressure after the first drop up to almost the same pressure level $p_2 \approx p_1$, if chorion ruptures first. These pressure versus time characteristics were in 75 % of the cases in agreement with the visual observations. As to the rupture position, it was distinguished whether the sample ruptured in the center,

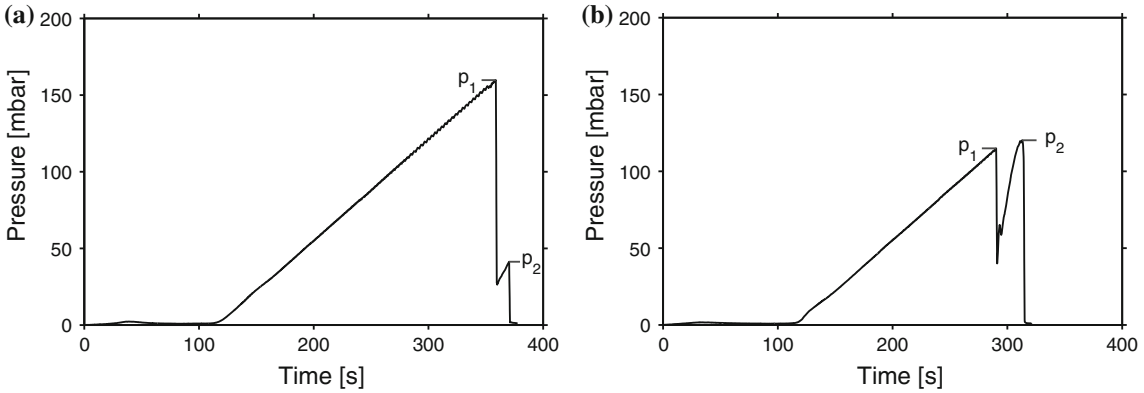

Fig. 5 Characteristic pressure versus time curves. **a** Amnion rupture first, characterized by $p_1 > p_2$. **b** Chorion rupture first, characterized by $p_1 \approx p_2$

27 cases, away from the clamping cover, 10 cases, or very close or at the clamping ring, 14 cases.

3.4 Influence of model formulations

Due to the non-homogeneous strain field within the FM samples, the biaxial tension–stretch parameters extracted from the experiments depend on the constitutive model formulation assumed for the inverse analysis. Different hyperelastic constitutive equations were applied and their influence on the correlations between mechanical and microstructural parameters investigated. Figure 3 illustrates the parameterized curves for the determination of λ_{plane}, as obtained using the different constitutive models. It is evident that the calculated stretch values converge for small deformations and moderate preinflation displacements, thus model formulation does not influence the low stretch stiffness value K_1. On the contrary, for large displacements, the λ_{plane} values predicted from the different models differ significantly, thus affecting K_2.

Figure 6 illustrates the dependence of the experimental high stretch stiffness values on the model formulations. There is a strong correlation between the values obtained from different model equations. The same is valid for λ_{crit}. Due to the proportionality between the corresponding mechanical parameters, the choice of the constitutive model influences the absolute values but not the existence of a correlation between mechanical and microstructural parameters. For the analyses of Sect. 2.7, the reduced polynomial model, based on the second invariant I_2, was chosen (Table 5).

3.5 Correlations between mechanical parameters and microstructural constituents

Coefficients of correlations were calculated between the microstructural data and the mechanical parameters, see Table 6. The small stretch stiffness K_1 does neither correlate

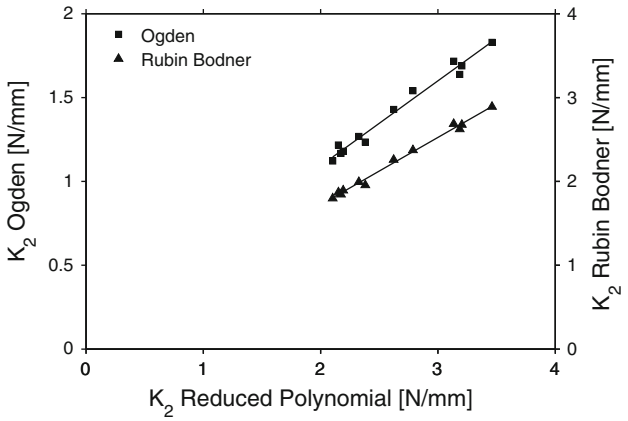

Fig. 6 Influence of constitutive model on the mechanical parameters determined for each FM, at the example of K_2

with the elastin content nor with the collagen content. There is a distinct correlation between the high stretch stiffness K_2 and the collagen content as well as between the critical membrane tension and the collagen content, Fig. 7. Furthermore, there is a pronounced proportionality between the mechanical data of high stretch stiffness, critical tension and maximum pressure, and the amount of PYD as well as DPD cross-links, as illustrated in Fig. 8. No correlation is present between elastin content and the values of membrane stiffness, critical tension, and critical stretch.

4 Discussion

This study demonstrates that under physiologic biaxial loading conditions, the high stretch stiffness as well as the strength of the fetal membrane depend on collagen content and its degree of cross-linking. In fact, a significant correlation could be found despite the variability and uncertainties associated with the determination of both, microstructural

Table 5 Mechanical parameters from the stress–strain curves

Membrane	K_1 (N/mm)	K_2 (N/mm)[a]	T_{crit} (N/mm)	λ_{crit} (−)[a]
1	0.072 ± 0.018	3.186 ± 1.165	0.403 ± 0.102	1.247 ± 0.022
2	0.073 ± 0.040	3.461 ± 1.000	0.301 ± 0.081	1.225 ± 0.036
3	0.139 ± 0.078	2.787 ± 0.947	0.267 ± 0.136	1.181 ± 0.012
4	0.129 ± 0.054	2.622 ± 0.680	0.199 ± 0.038	1.145 ± 0.019
5	0.153 ± 0.013	3.134 ± 1.009	0.272 ± 0.099	1.169 ± 0.009
6	0.134 ± 0.128	2.173 ± 0.687	0.243 ± 0.071	1.181 ± 0.021
7	0.061 ± 0.014	2.381 ± 0.096	0.259 ± 0.079	1.253 ± 0.042
8	0.084 ± 0.026	2.152 ± 0.168	0.149 ± 0.012	1.156 ± 0.014
9	0.103 ± 0.042	2.193 ± 0.228	0.220 ± 0.052	1.195 ± 0.018
10	0.114 ± 0.032	2.325 ± 0.358	0.211 ± 0.019	1.182 ± 0.011
11	0.076 ± 0.009	2.103 ± 0.245	0.204 ± 0.043	1.198 ± 0.026
12	0.117 ± 0.037	3.204 ± 0.459	0.342 ± 0.100	1.207 ± 0.014

Values are membrane-specific averages. The number of samples per membrane can be found in Table 1

[a] The absolute values of these parameters depend on the constitutive model adopted for the inverse analysis

Table 6 Coefficients of correlation R between microstructure and mechanical parameters

	Collagen	Elastin	PYD	DPD	Thickness
K_1	−0.207	−0.004	−0.099	−0.140	0.119
K_2	**0.689**	0.263	**0.824**	**0.764**	−0.460
T_{crit}	**0.705**	0.390	**0.760**	**0.801**	−0.160
p_{max}	**0.808**	0.432	**0.741**	**0.740**	−0.314
λ_{crit}	0.527	0.242	0.439	0.514	−0.098

Values in bold are statistically significant ($p < 0.05$)

and mechanical parameters. Due to these uncertainties, it is important to compare parameter values obtained in the present work with corresponding findings reported in the literature.

4.1 Histological and biochemical data

Reported values for the collagen content of intact fetal membranes, range from 4 to 20 % (Hampson et al. 1997; Jabareen et al. 2009) of dry weight, which is in line with the present value of 18.4 ± 4.9 % DW. The amount of elastin in the present work was determined as 17.6 ± 1.9 % DW. This result agrees with the one obtained in Jabareen et al. (2009) in terms of average and variability, if the present values are expressed as percentage of wet weight (2.5 ± 0.44 % WW vs. 2.1 ± 0.72 % WW), but differs evidently from the 0.08 % of fat-free dry weight (Hieber et al. 1997) or 36 % of (total) wet weight of fresh amnion (Wilshaw et al. 2006). Note that accounting for scatter in water content significantly increases the variability of the data. Deviations in the elastin content can be explained by the difficulty of its extraction and measurement using biochemical methods. There is only one study by Stuart et al. (2005) reporting values of pyridinoline and deoxypyridinoline cross-links in human amnion. The reported pyridinoline concentrations range from 7.9 to 8.3 nmol/µmol hydroxiproline and the corresponding values of deoxypyridinoline from 0.26 to 1.02 nmol/µmol hydroxiproline, giving an average PYD/DPD ratio of 18.4. Our findings of averaged PYD and DPD contents of 4,766 ± 3,125 nmol/l and 233 ± 191 nmol/l, respectively, can hardly be compared since they result from measurements on intact membranes. Nevertheless, our presented average PYD/DPD ratio of 23.8 ± 5.7 is in good agreement with Stuart et al. (2005).

Pyrodinoline cross-links are a mature form of cross-link associated with collagen I, but not with collagen type IV, Avery and Bailey (2008), Eyre and Wu (2005). These cross-links occur between tropocollagens to form fibrils and also between fibrils for higher level organization. Type IV collagen contains ketoamine (immature) and disulfide cross-links, not quantified in this study. Tissues with high collagen turnover, and in particular fetal tissues, contain larger amounts of immature cross-links (also for fibrillar collagen). Immature cross-links are thus expected to be relevant in this tissue, as part of type IV collagen as well as in developing fibrillar collagen. A full rationalization of mechanical behavior would require a description of cross-linking maturity.

4.2 Mechanical parameters

A direct comparison of the determined mechanical parameters with the corresponding values reported in the literature is often difficult due to differences in the experimental setup and procedure. Most of the previous work with inflation experiments focussed on the determination of the strength of the FM, so that often only values of burst pressure (MacLachlan 1965) or maximum deflection (Parry-Jones and Priya 1976; Al-Zaid et al. 1980) were determined. These

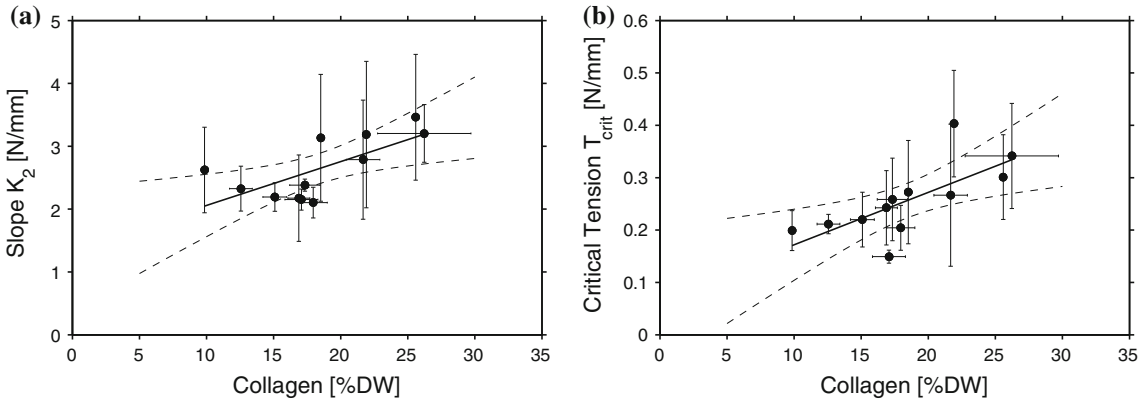

Fig. 7 Correlations between microstructure and mechanics. **a** Correlation between collagen content and high stretch stiffness K_2, **b** correlation between collagen content and critical membrane tension. *Solid line*: regression line, *dashed line*: 95 % confidence interval

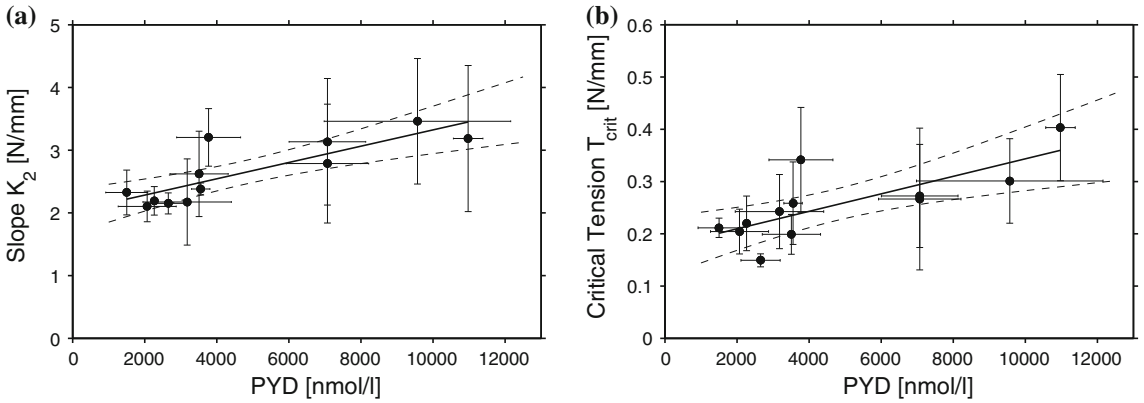

Fig. 8 Correlations between microstructure and mechanics. **a** correlation between content of PYD cross-links and high stretch stiffness K_2, **b** correlation between PYD cross-links and critical membrane tension. *Solid line*: regression line, *dashed line*: 95 % confidence interval

values cannot be compared with the present data, since they depend on the size of the FM sample. Using Laplace's law, Polishuk et al. (1962) and Lavery and Miller (1979); Lavery et al. (1982) determined the critical stress at rupture and the critical membrane tension in their inflation experiments. The membrane's "stress tolerance" in Lavery et al. (1982) can be converted, with the assumption of an average membrane thickness of 0.5 mm, to a critical membrane tension, providing values between 0.37 and 0.45 N/mm. Polishuk determined the critical membrane tension to be 0.205 N/mm which is in good agreement with the herein determined value of 0.256 ± 0.069 N/mm which in contrast is considerably higher than the maximum membrane tension of 0.035 N/mm determined by Joyce (2009), based on planar biaxial tests. More information on material-specific mechanical parameters can be found if the literature based on uniaxial tensile tests is taken into account, since this test configuration is easier to analyze. For parameters comparable to the present high stretch stiffness K_2, values range from 0.87 N/mm (Oxlund et al. 1990) to 0.92 N/mm (Jabareen et al. 2009) up to 1.35 N/mm (Helmig et al. 1993). These values are significantly lower than the present biaxial stiffness K_2 of 2.64 ± 0.49 N/mm. Maximum uniaxial membrane tension has often been characterized, leading to values of 0.15 N/mm (Jabareen et al. 2009), 0.25 N/mm (Oxlund et al. 1990), 0.36 N/mm (Helmig et al. 1993), 0.44–0.85 N/mm (Artal et al. 1976), and 0.98 N/mm (Artal et al. 1979). Our finding of the average critical tension of 0.256 ± 0.069 N/mm is within the reported ranges. In agreement with the study of Schober et al. (1994a), no correlation between the sample thickness and the mechanical parameters characterizing strength and ductility could be found. The initial stiffness of $9.1 \pm 1.9 \times 10^{-3}$ N/mm from our previous uniaxial study (Jabareen et al. 2009) was considerably lower than the present value of $105 \pm 31 \times 10^{-3}$ N/mm. In the same way, the average critical deformation or strain at rupture from this study with a value of 19.5 ± 3.4 % is significantly smaller compared to uniaxial studies, obtaining values around 50 % (Prevost 2004; Helmig et al. 1993; Jabareen et al. 2009) or even up to 70–100 % (Artal et al. 1976, 1979). An improved setup for inflation experiments is currently being developed using an additional camera placed above the sample and a

Table 7 Comparison of the mechanical parameters from the stress–strain curves for different constitutive models

	K_2 (N/mm)	λ_{crit} (–)
Reduced polynomial	2.643 ± 0.492	1.195 ± 0.034
Rubin Bodner	2.239 ± 0.397	1.217 ± 0.040
Ogden	1.419 ± 0.252	1.299 ± 0.067

light source within the cylinder, with and without additional markers on the membrane. Extraction of local strain fields in preliminary experiments proved difficult due to membranes inhomogeneity leading to a complex displacement field. Digital image correlation was used to determine radial and circumferential displacement at the boundaries of a "central region," from which an "average" biaxial strain can be extracted for the apex. The failure strain measured at the apex in these preliminary investigations was around 20 %. Furthermore, Joyce (2009) determined the maximum areal strain in planar biaxial tests to be 0.6 ± 0.03, which corresponds to 26 % in-plane strain according to our definition. This difference between uniaxial and biaxial initial stiffness and critical deformation is related to the larger compliance observed in uniaxial tensile tests, which might be associated with significant re-orientation of collagen fibers. In contrast, as demonstrated by Joyce (2009), a biaxial state of stress causes only a slight increase in fiber alignment in the amnion layer for small pressure loads and no change in fiber orientation thereafter, thus leading to a reduction in the deformation capacity and to an initially stiffer response.

As shown in Sect. 3.4, the membrane-specific values of the mechanical parameters K_2 and λ_{plane} in Table 5 depend on the constitutive model formulation used for the analysis of the inflation experiment. Table 7 reports the averages of these parameters for each of the model equation investigated. The differences are in the order of 15 % of the respective parameters, except the high stretch stiffness which shows the strongest dependence on constitutive model formulation, with a deviation >50 % between the Ogden model and the other formulations. The side view profile of selected membranes was analyzed and the contour (as well as the area enclosed within the contour) compared with corresponding finite element model predictions. Good agreement between calculations and measurements was obtained with the reduced polynomial and with the Rubin–Bodner model, whereas the predictions using the Ogden model did not match well the data. The correlation coefficients reported in Table 6 were calculated for the reduced polynomial I_2 model, but corresponding evaluations using the other models lead to similar results.

Inhomogeneity and imperfections in the tissue cause variations in the measurements within one membrane as well as between membranes from different donors, as illustrated in Fig. 4. A quantitative measure of the variation is the variance.

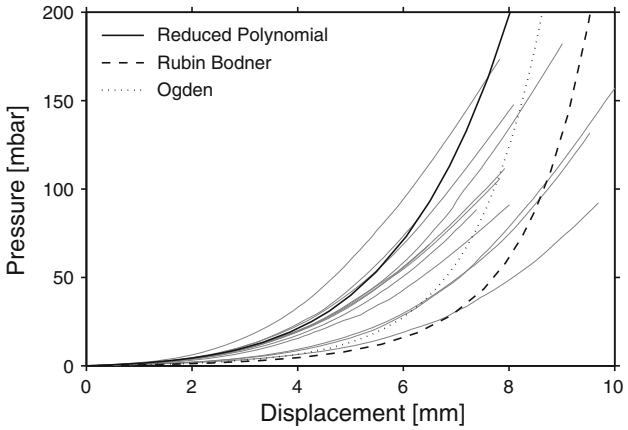

Fig. 9 Pressure–apex displacement curves from inflation experiments on fetal membranes (mean curves, thin gray). Predictions based on average stress–strain data of uniaxial tests, continuous line reduced polynomial model in I_2, *dashed line* Rubin Bodner model in I_1 and dotted line Ogden model in the principal stretches. The simulation results have been obtained by the use of the parameters in Table 2

Calculation of the intra (within one membrane) and inter (within averages from different membranes) variance enables the assessment of the accuracy of the measurements. For the present study, the intra variance of the mechanical parameters characterizing the strength, stiffness, and ductility ranges from 10 to 26 % and the corresponding inter variance from 18 to 33 %. For the study of Schober et al. (1994a), the intra variance is 16–34 % and the inter variance 10–60 %, evaluated for the same mechanical parameters. For our previous uniaxial study (Jabareen et al. 2009), the corresponding variances are 7–21 and 55–63 %, respectively. The variance of the present study is at the lower limit of the reported ranges, confirming the reliability of the experimental setup and the procedures used for data analysis.

4.3 Mechanical behavior of FM

The model formulations used for the analysis of the present data can be fitted also to corresponding uniaxial stress experiments (Jabareen et al. 2009). Both the I_1 and principal stretch-based model equations (with parameters selected to fit the average uniaxial response) largely underestimate the resistance to deformation in inflation experiments, see Fig. 9. Better predictions are obtained when the model formulation is based on the second invariant I_2 of the Cauchy-Green deformation tensor $\mathbf{C}$. It can be shown that I_1 is proportional to the average (squared) stretch of the sides of an infinitesimal volume element, whereas I_2 is proportional to the average area stretch of the faces of an infinitesimal volume element. The fact that fetal membrane behaves as a I_2 material might be associated with the network-like arrangement of the collagen, suggesting a response similar to that of a textile, with

much higher resistance to changes in the area (in the plane of the membrane) than to elongations in a uniaxial state of stress.

Miller et al. (1979) optimized a Mooney material, which includes per definition the first and second invariant of **C**, on the response of FM. They report that each value of C_2, the multiplier of I_2, was 0.1 times the value of C_1. Based on the corresponding strain energy formulation and the assumption of an average membrane thickness of 0.5 mm, the initial slope of the tension–stretch curve can be calculated. The corresponding values range from 0.066 up to 0.99 N/mm with a population peak at 0.33 N/mm. Our finding of an average low stretch stiffness of K_1 0.105 ± 0.031 N/mm is in line with these data.

Prevost (2004) and Joyce (2009) optimized structural constitutive models on the biaxial response of FM. Prevost worked with a square unit cell model consisting of four individual chains, where each chain represents a collagen fibril and has a simple force–stretch relationship. He achieved a good prediction of the uniaxial response but failed to capture the initial compliant response under biaxial stress. The structural constitutive models used by Joyce (2009) based on the tissue behavior on the fiber level and included a statistical distribution of the fiber recruitment. Those models fitted well the biaxial response of FM. It is interesting to note that both, Prevost and Joyce, worked with experimental stress–strain curves which were characterized by no initial stiffness, since they have chosen an non-pre-stretched reference configuration in their experiments. As a consequence, Prevost's simulation could only be related to the experimental data after a corresponding horizontal shift. Joyce overcomes this problem by the introduction of a so-called slack strain, which characterizes the initial undulation of the tissue.

4.4 Correlation between mechanical and microstructural parameters

The high stretch stiffness as well as the critical membrane tension were found to be proportional to collagen content and the concentrations of the PYD and DPD cross-links. Multiple linear regression analysis shows that the cross-links and collagen content do not correlate independently with mechanical parameters. Since mature cross-links (PYD and DPD) are associated only with fibrillar collagen in its mature form, this finding might indicate that total collagen is predominantly made of fibrillar collagen. The values reported in Table 6 show somewhat larger correlation between membrane mechanical parameters (high strain stiffness, K_2, and critical tension, T_{crit}) and pyrodinoline cross-links. A lower correlation for the cross-links would have indicated an important contribution of non-fibrillar collagen to mechanical parameters. Thus, the present observations do not support previous hypotheses (Moore et al. 2006; Bachmaier and Graf 1999) which attributed to collagen type IV a significant role in mechanical strength of fetal membranes. Collagen type IV contributes to fetal membranes microfibrils complex (Malak et al. 1993; Bachmaier and Graf 1999) which might influence small strain deformation behavior. The absence of correlation between K_1 and collagen content might be due to the lower amount of type IV in total collagen as compared to fibrillar collagen. Quantitative determination of each collagen type, as well as divalent and ketoamine cross-links would enable identifying the contribution of fibrillar and non-fibrillar collagen to the mechanical behavior of fetal membranes.

The organization of collagen fibrils in loose bunches, not forming higher-order bundles, determines the deformability of fetal membranes. In this sense, it is interesting to compare mechanical and microstructural characteristics of amnion and liver capsule, see Hollenstein (2011). Although the amnion contains a similar amount of collagen (per dry weight) compared to liver capsule, and it is of the same thickness, it is much softer than the capsule. The difference is related to the fact that, in contrast to amnion, collagen in liver capsule forms thicker (4–6 μm) fiber bundles.

In contrast to our previous observations from uniaxial stress tests, Jabareen et al. (2009), no correlation could be observed between the elastin content and low stretch resistance to deformation. This discrepancy might be interpreted with respect to the role of microstructure constituents in deformation behavior. We hypothesize that in the case of uniaxial stress, collagen fibers are re-oriented at low strains, such that resistance to deformation is provided by the elastin matrix. On the other hand, in case of a biaxial state of stress, collagen fibers contribute to low deformation resistance, in that the initially crimped collagen fibers are straighten in all directions of the membrane plane, without major global re-orientation. The mechanisms of progressive fiber recruitment and un-crimping and its relationship with the highly nonlinear tissue response (leading to the transition from low-to-higher stiffness) are well described in the literature (Lanir 1983; Sacks and Wei 2003; Hill et al. 2012). We propose that, for the uniaxial stress state, low strain compliance is enhanced by global fiber re-orientation. An additional argument supporting this interpretation is the observed higher values of low stretch stiffness K_1 in the biaxial state of stress compared to a uniaxial stress state. On the other hand, it should be noted that the low stretch stiffness value strongly depends on the definition of a reference configuration (the normalization of the pressure–displacement curves at a preload of 1 mbar in the present case, or the threshold force value used in uniaxial tensile stresses). Further, low stretch stiffness values are also influenced by the history dependence of the FM mechanical response, and no preconditioning was applied in the present experiments.

Table 8 Coefficients of correlation R between mechanical and biochemical parameters

	Collagen	Elastin	PYD	DPD
K_2*	0.394	0.134	**0.679**	**0.590**
λ_{crit}*	0.337	0.138	0.138	0.223

The mechanical parameters, denoted with *, have been obtained without the use of the normalization criterion. Values in bold are statistically significant ($p < 0.05$)

4.5 Rupture behavior

Concerning the rupture sequence of FM, it was observed in this study that the amnion ruptures first in 73 % of the cases. The results in terms of rupture sequence in mechanical testing depend on the experimental procedures. Artal et al. (1976), Lavery and Miller (1977), and Arikat et al. (2006) found that chorion ruptures first. In contrast, Schober et al. (1994b), Helmig et al. (1993), and Oxlund et al. (1990) observed that amnion ruptures first. Differences in the rupture sequence are likely to be due to the loading configuration (uniaxial tension, puncture test, inflation) and probably also to artifacts related to sample fixation. In that regard, we consider the present experimental setup more reliable in that biaxial loading is induced by fluid pressure and membrane rupture mostly occurred away from the clamping.

4.6 Importance of normalization

In order to obtain accurate mechanical measurements, it is essential to reliably define a reference configuration. According to Sect. 2.4, we define the start of the measurement as the point where the difference between the measured total pressure and the hydrostatic pressure of the fluid column is equal to 1 mbar, which provides the deformed reference configuration. According to this pressure preload, the average initial membrane tension is 2.06×10^{-3} N/mm, which is less than 1 % of the critical membrane tension. The corresponding strain at normalization is less than 2 %, if estimated with the average low stretch stiffness. If this normalization criterion would not be applied (in fact, this step is usually omitted in literature), the reference configuration would be assumed to be a flat membrane. Resulting from this assumption, the membrane deformations would be clearly higher. The critical stretch at membrane rupture would change from 1.195 ± 0.034 to 1.431 ± 0.079 and the high stretch stiffness reduces from 2.64 ± 0.49 to 1.88 ± 0.41 N/mm. In addition, as illustrated in Table 8, all coefficients of correlations would be reduced and the demonstrated relationship between mechanical and microstructural data could not be obtained anymore. The reason for this is in the higher variability of the mechanical data, caused by uncertainties in the initial configuration. The handling of soft biological tissues prior to mechanical testing is user subjective and even if done with great care, small wrinkles in the tissue or clamping the tissue under slight tension can never be totally excluded. On that account, the definition of a suitable reference configuration cannot be over emphasized.

4.7 Clinical relevance of findings

There are several studies covering the biochemical characteristics of premature ruptured membranes (PROM). Skinner et al. (1981) report a significantly lower collagen content in the amnion from PROM membranes compared to membranes ruptured at term. In contrast, MacDermott and Landon (2000) found that there is no generalized reduction of the collagen content in the amnion and hypothesizes that PROM is caused by a localized membrane weakness. Apart from that, both studies report a decrease of the collagen content, in the amnion layer, with progressing gestational age. More recent, Stuart et al. (2005) confirmed the reduced collagen content in prelabor membranes, but found no difference in the collagen content between samples from the rupture site and the non-rupture site. Furthermore, there was no difference in the collagen cross-link profile between the PROM and control group, but there was a regional variation in the cross-link ratio (PYD/DPD) for samples from the rupture site. Stuart et al. (2005) conclude that collagen cross-linking is not involved in the etiology of PROM, but that the formation of rupture initiation is a function of the regional variation in the cross-link ratio. Our results clearly indicate that a weakening of the membrane is expected if the collagen content is reduced or less cross-links are present. This supports the hypothesis that PROM might be caused by a (local) decrease in resistance of the collagen fiber network.

5 Conclusions

This study represents the continuation of our efforts to quantitatively analyze the relationship between microstructure and nonlinear deformation behavior of FM and provide further understanding of the mechanical behavior of FM. Biochemical assays were used to quantify the content of elastin and total collagen and concentrations of pyridinoline and deoxypyridinoline cross-links were determined by HPLC measurement. Low and high stretch tangent modules (K_1 and K_2), critical membrane tension (T_{crit}), and stretch (λ_{crit}) at rupture were determined using a finite element-based procedure for the analysis of the measurements in the inflation experiments. The influence of the constitutive model formulation on the results of this analysis has been investigated. FM was shown to behave as I_2 material, that is a material with higher resistance to area change as compared to elongation with

free lateral contraction. Correlations were found between the microstructural data and mechanical parameters: there is a distinct relationship between the microstructural data of total collagen content and the concentrations of PYD as well as DPD cross-links, and the mechanical parameters of high stretch stiffness as well as critical tension. No correlation was found between the elastin content and the low stretch stiffness, in contrast to a previous uniaxial study.

Immature (ketoamine and disulfide) cross-links are expected to be relevant in this fetal tissue, as part of type IV collagen as well as in developing fibrillar collagen. Quantitative assessment of cross-linking maturity is expected to provide relevant contributions toward a full rationalization of the mechanical behavior of fetal membranes. The most important improvement for future inflation experiments concerns the introduction of a system for image-based strain measurement at the apex of the inflated membrane. Improved illumination might enable to extract the displacement field from the side view profile, as realized in Myers et al. (2010). The experimental procedure is currently being improved with an additional camera view from above the membrane and a corresponding procedure for strain measurement based on digital image correlation. In this way, uncertainties related to constitutive model formulation will be eliminated for the quantitative determination of mechanical parameters from inflation test measurements.

Acknowledgments The authors gratefully acknowledge financial support by the Swiss National Science Foundation project nr. 3200B-124925/1.

References

ABAQUS (2006) Abaqus analysis user's manual, 6th ed. Abaqus Inc., RI

Al-Zaid NS, Bou-Resli MN, Goldspink G (1980) Bursting pressure and collagen content of fetal membranes and their relation to premature rupture of the membranes. Br J Obstet Gynaecol 81(3):227–229

Arikat S, Novince RW, Mercer BM, Kumar D, Fox JM, Mansour JM, Moore JJ (2006) Separation of amnion from choriodecidua is an integral event to the rupture of normal term fetal membranes and constitutes a significant component of the work required. Am J Obstet Gynecol 194(1):211–217

Artal R, Sokol RJ, Neuman M, Burstein AH, Stojkov J (1976) The mechanical properties of prematurely and non-prematurely ruptured membranes. Am J Obstet Gynecol 125(5):655–659

Artal R, Burgeson RE, Hobel CJ, Hollister D (1979) An in vitro model for the study of enzymatically mediated biomechanical changes in the chorioamniotic membranes. Am J Obstet Gynecol 133(6):656–659

Avery NC, Bailey AJ (2008) Restraining cross-links responsible for the mechanical properties of collagen fibers: natural and artificial, vol 26. Springer, Berlin, pp 81–110

Bachmaier N, Graf R (1999) The anchoring zone in the human placental amnion: bunches of oxytalan and collagen connect mesoderm and epithelium. Anat Embryol 200(1):81–90

Beck V, Lewi P, Gucciardo L, Devlieger R (2011) Preterm prelabor rupture of membranes and fetal survival after minimally invasive fetal surgery: a systematic review of the literature. Fetal Diagn Ther 31:1–9

Bryant-Greenwood GD (1998) The extracellular matrix of the human fetal membranes: structure and function. Placenta 19(1):1–11

Calvin S, Oyen M (2007) Microstructure and mechanics of the chorioamnion membrane with an emphasis on fracture properties. In: Reproductive biomechanics. Ann NY Acad Sci, vol 1101. Blackwell, England, pp 166–185

Canny J (1986) A computational approach to edge detection. IEEE Trans Pattern Anal Mach Intell 8(6):679–698

Demiray H (1972) A note on the elasticity of soft biological tissues. J Biomech 5(3):309–311

El Khwad M, Stetzer B, Moore RM, Kumar D, Mercer B, Arikat S, Redline RW, Mansour JM, Moore JJ (2005) Term human fetal membranes have a weak zone overlying the lower uterine pole and cervix before onset of labor. Biol Reprod 72(3):720–726

Eyre DR, Wu JJ (2005) Collagen cross-links. Top Curr Chem 247:207–229

Hampson V, Liu D, Billett E, Kirk S (1997) Amniotic membrane collagen content and type distribution in women with preterm premature rupture of the membranes in pregnancy. Br J Obstet Gynaecol 104:1087–1091

Helmig R, Oxlund H, Petersen LK, N U (1993) Different biomechanical properties of human fetal membranes obtained before and after delivery. Eur J Obstet Gynecol Reprod Biol 48(3):183–189

Hieber AD, Corcino D, Motosue J, Sandberg LB, Roos PJ, Yu SY, Csiszar K, Kagan HM, Boyd CD, Bryant-Greenwood GD (1997) Detection of elastin in the human fetal membranes: proposed molecular basis for elasticity. Placenta 18(4):301–312

Hill MR, Duan X, Gibson GA, Watkins S, Robertson AM (2012) A theoretical and non-destructive experimental approach for direct inclusion of measured collagen orientation and recruitment into mechanical models of the artery wall. J Biomech 45(5):762–771

Hollenstein M (2011) Mechanics of the human liver: experiments and modeling. PhD thesis, Swiss Federal Institute of Technology Zurich

Ilancheran S, Moodley Y, Manuelpillai U (2009) Human fetal membranes: a source of stem cells for tissue regeneration and repair?. Placenta 30(1):2–10

Jabareen M, Mallik AS, Bilic G, Zisch AH, Mazza E (2009) Relation between mechanical properties and microstructure of human fetal membranes: an attempt towards a quantitative analysis. Eur J Obstet Gynecol Reprod Biol 144(Suppl):S134–S141

Joyce E (2009) Micromechanical mechanisms of fetal membrane failure. PhD thesis, University of Pittsburgh

Joyce E, Moore J, Sacks M (2009) Biomechanics of the fetal membrane prior to mechanical failure: review and implications. Eur J Obstet Gynecol Reprod Biol 144:121–127

LabView (2008) LabView manual, National Instruments, USA

Lanir Y (1983) Constitutive equations for fibrous connective tissues. J Biomech 16(1):1–12

Lavery J, Miller C (1977) The viscoelastic nature of chorioamniotic membranes. Obstet Gynecol 50(4):467–472

Lavery J, Miller C (1979) Deformation and creep in the human chorioamniotic sac. Am J Obstet Gynecol 134(4):366–375

Lavery J, Miller C, Knight R (1982) The effect of labor on the rheologic response of chorioamniotic membranes. Obstet Gynecol 60(1):87–92

MacDermott RI, Landon CR (2000) The hydroxyproline content of amnion and prelabour rupture of the membranes. Eur J Obstet Gynecol Reprod Biol 92(2):217–221

MacLachlan T (1965) A method for the investigation of the strength of the fetal membranes. Am J Obstet Gynecol 91(3):309–313

Malak TM, Ockleford CD, Bell SC, Dalgleish R, Bright N, Macvicar J (1993) Confocal immunofluorescence localization of

collagen types i, iii, iv, v and vi and their ultrastructural organization in term human fetal membranes. Placenta 14(4):385–406
MATLAB (2010) The Mathworks, Matlab Documentation, Version 7.10.0 (R2010a). The Mathworks Inc
Meinert M, Eriksen GV, Petersen AC, Helmig RB, Laurent C, Uldbjerg N, Malmstrm A (2001) Proteoglycans and hyaluronan in human fetal membranes. Am J Obstet Gynecol 184(4):679–685
Mercer B (2003) Preterm premature rupture of the membranes. Obstet Gynecol 101(1):178–193
Miller C, Lavery J, Donnelly T (1979) Determination of elastic parameters for human fetal membranes. J Rheol 23(1):57–78
Moore RM, Mansour JM, Redline RW, Mercer BM, Moore JJ (2006) The physiology of fetal membrane rupture: insight gained from the determination of physical properties. Placenta 27(11–12):1037–1051
Myers KM, Cone FE, Quigley HA, Gelman S, Pease ME, Nguyen TD (2010) The in vitro inflation response of mouse sclera. Exp Eye Res 91(6):866–875
Ogden RW (1972) Large deformation isotropic elasticity—on the correlation of theory and experiment for incompressible rubberlike solids. Proc R Soc Lond 326:565–584
Oxlund H, Helmig R, Halaburt JT, Uldbjerg N (1990) Biomechanical analysis of human chorioamniotic membranes. Eur J Obstet Gynecol Reprod Biol 34(10):247–255
Oyen M, Cook R, Stylianopoulos T, Barocas V, Calvin S, Landers D (2005) Uniaxial and biaxial mechanical behavior of human amnion. J Mater Res 20(11):2902–2909
Parry-Jones E, Priya S (1976) A study of the elasticity and tension of fetal membranes and of the relation of the area of the gestational sac to the area of the uterine cavity. Br J Obstet Gynaecol 83(3):205–212
Polishuk W, Peranio A, Kohane S (1962) The physical properties of fetal membranes. Obstet Gynecol 20(2):204–210
Prevost TP (2004) Biomechanics of the human chorioamnion. Master thesis, Dep Mater Sci Eng, Massachusetts Institute of Technology
Rivlin RS, Saunders DW (1951) Large elastic deformations of isotropic materials. vii. Experiments on the deformation of rubber. Phil Trans Math Phys Eng Sci 243(865):251–288
Rubin MM, Bodner SR (2002) A three-dimensional nonlinear model for dissipative response of soft tissue. Int J Solid Struct 39(19):5081–5099
Sacks M, Wei S (2003) Multiaxial mechanical behavior of biological materials. Annu Rev Biomed Eng 5(1):251–284
Schober E, Kusy R, Whitley J, Savitz D (1994a) Effect of thickness on the fracture characteristics of fetal membranes. J Mater Sci Mater Med 5(3):130–137
Schober EA, Kusy RP, Savitz DA (1994b) Resistance of fetal membranes to concentrated force applications and reconciliation of puncture and burst testing. Ann Biomed Eng 22(5):540–548
Skinner SJ, Campos GA, Liggins GC (1981) Collagen content of human amniotic membranes: effect of gestation length and premature rupture. Obstet Gynecol 57(4):487–489
Stuart EL, Evans GS, Lin YS, Powers HJ (2005) Reduced collagen and ascorbic acid concentrations and increased proteolytic susceptibility with prelabor fetal membrane rupture in women. Biol Reprod 72(1):230–235
Wilshaw SP, Kearney JN, Fisher J, Ingham E (2006) Production of an acellular amniotic membrane matrix for use in tissue engineering. Tissue Eng 12(8):2117–2129
Wittenberg GF (2011) Elastic properties and yield stress of fetal membranes. Conference proceedings: annual international of the IEEE engineering in medicine and biology society. pp 2123–2126